Electronic Supplementary Information

Penta-OsP_2 and Penta-RhS_2 Sheets Derived from Marcasite and Pyrite with Low Lattice Thermal Conductivity

Yiheng Shen,[a] Jie Sun,[a] Yanyan Chen,[a] Dongyuan Ni,[a] Tingwei Li,[a] Akira Yoshikawa,[b] Yoshiyuki Kawazoe,[c] and Qian Wang*[a]

[a] CAPT, School of Materials Science and Engineering, BKL-MEMD, Peking University, Beijing 100871, China.

[b] Institute for Materials Research, Tohoku University, Sendai, 980-8577, Japan;

[c] New Industry Creation Hatchery Center, Tohoku University, Sendai, 980-8577, Japan; Department of Physics, Suranaree University of Technology, 30000 Nakhon Ratchasima, Thailand; Department of Physics and Nanotechnology, SRM Institute of Science and Technology, Kattankulathur, Tamil Nadu 603203, India.

* Author to whom any correspondence should be addressed: qianwang2@pku.edu.cn

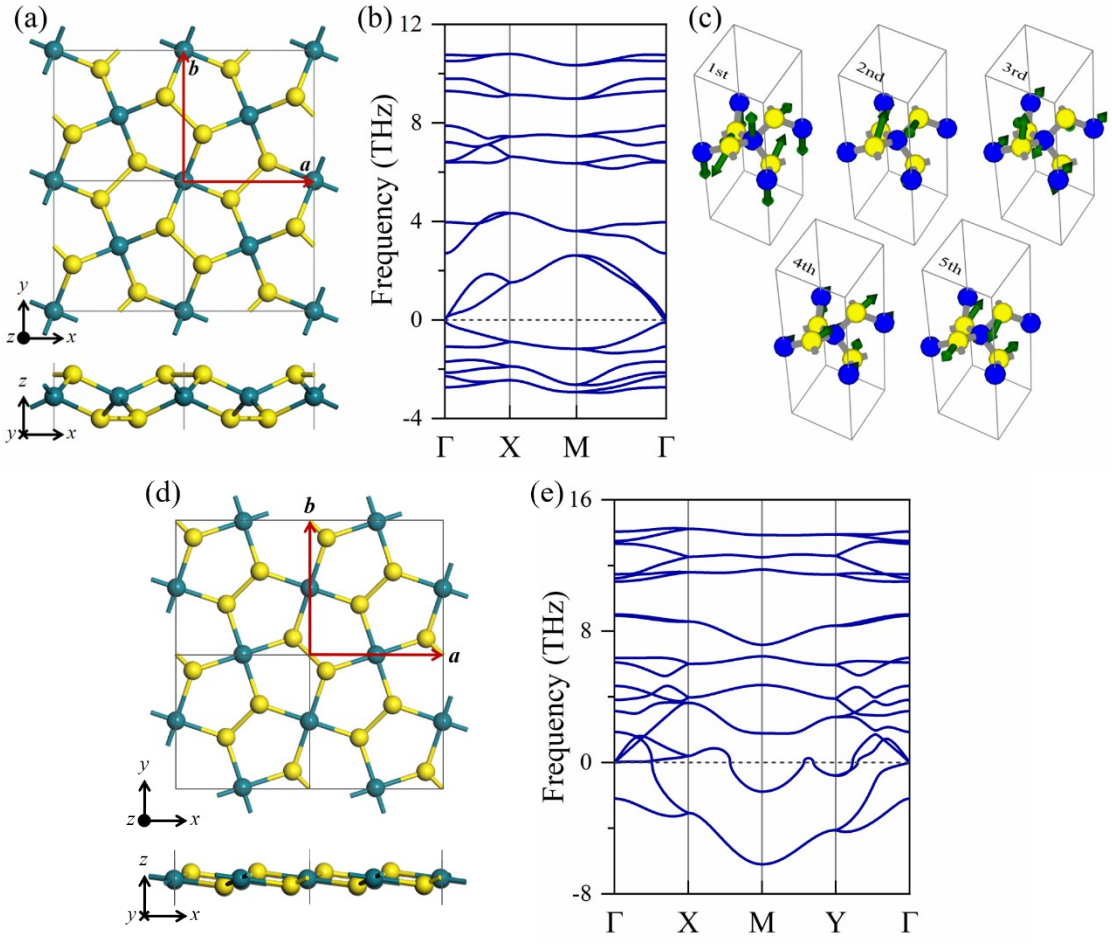

Fig. S1 (a) Geometry, (b) phonon band structure, and (c) imaginary phonon modes of the tetragonal RhS_2 sheet with the penta-CN_2 configuration. (d) Geometry and (e) phonon band structure of the orthorhombic RhS_2 sheet with the penta-$PdSe_2$ configuration.

Text S1 Thermal stability of penta-RhS_2 at 600 K

We perform an AIMD simulation for a 3×3×1 supercell of the penta-RhS_2 primitive cell under the NPT ensemble (600 K and 100 kPa) for a simulation time of 10 ps with a time step of 1 fs. The variation of the supercell size with the simulation time is plotted in Fig. S2(a). We use the average lattice parameters from the last 5 ps as the reasonable size of the supercell for the following up NVT simulation at 600 K. The lattice parameter *a* (*b*) slightly shrinks from the original value of 13.41 Å to 13.32 (13.12) Å

due to the expansion in the out-of-plane direction. As shown in Fig. S2(b), the total potential energy shifts toward a lower energy level during the NVT simulation, which is consistent with our original result that penta-RhS_2 is thermally unstable above 500 K.

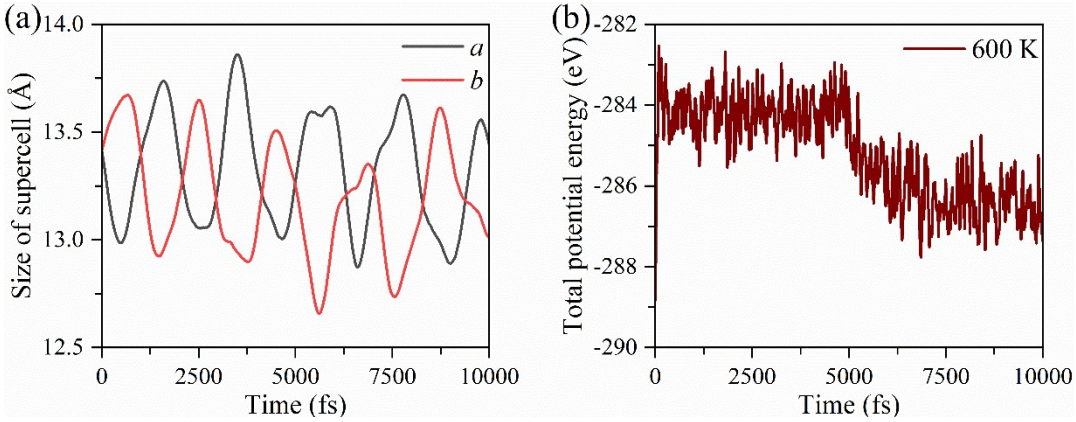

Fig. S2 Vibration of (a) the size of penta-RhS_2 supercell in NPT simulation, and (b) the total potential energy of the supercell in NVT simulation with simulation time.

Text S2 Mechanical properties of penta-OsP_2 of and penta-RhS_2

We calculate the Young's modulus E and Poisson's ratio ν of penta-OsP_2 and penta-RhS_2 from their stiffness tensor components C_{ij} based on the following equations:

$$E(\theta)=\frac{C_{11}C_{22}-C_{12}^2}{C_{11}s^4+C_{22}c^4+\left(\frac{C_{11}C_{22}-C_{12}^2}{C_{66}}-2C_{12}\right)s^2c^2}, \quad \text{(S1)}$$

and

$$\nu(\theta)=\frac{C_{12}\left(s^4+c^4\right)-\left(C_{11}+C_{22}-\frac{C_{11}C_{22}-C_{12}^2}{C_{66}}\right)s^2c^2}{C_{11}s^4+C_{22}c^4+\left(\frac{C_{11}C_{22}-C_{12}^2}{C_{66}}-2C_{12}\right)s^2c^2}, \quad \text{(S2)}$$

where θ is the angle between a specific in-plane direction and the crystalline orientation [100], $s = \sin\theta$, and $c = \cos\theta$. The calculated results are plotted in Fig. S2. The Young's

modulus of penta-OsP_2 exhibits strong anisotropy. The Young's modulus along the stiffer x axis (94.96 GPa·nm) is three times larger than that along the y axis (29.14 GPa·nm), while a maximal value of 105.06 GPa·nm is found at θ = 24° and its equivalents, which coincide with the [210] direction in penta-OsP_2. In contrast, the Young's modulus of penta-RhS_2 shows weak anisotropy along the axial directions x (65.18 GPa·nm) and y (61.76 GPa·nm), with a minimal Young's modulus of 30.86 GPa·nm found at θ = 45°. It is worth mentioning that, while materials with similar geometric structure and heavier atoms tend to have lower Young's modulus, penta-OsP_2 and penta-RhS_2 serve as a counter example where penta-OsP_2 with heavier Os atom is stiffer along most directions.

The Poisson's ratios of penta-OsP_2 of and penta-RhS_2 along the axial directions also show strong and weak anisotropy, respectively. The Poisson's ratio of penta-OsP_2 has its maximum value of 0.56 along the x axis and its minimum value of −0.24 at θ = 41°, corresponding to the [110] direction in penta-OsP_2. While, the maximum (0.61) and minimum (0.19) of the Poisson's ratios of penta-RhS_2 are found at θ = 44° and 90°, respectively.

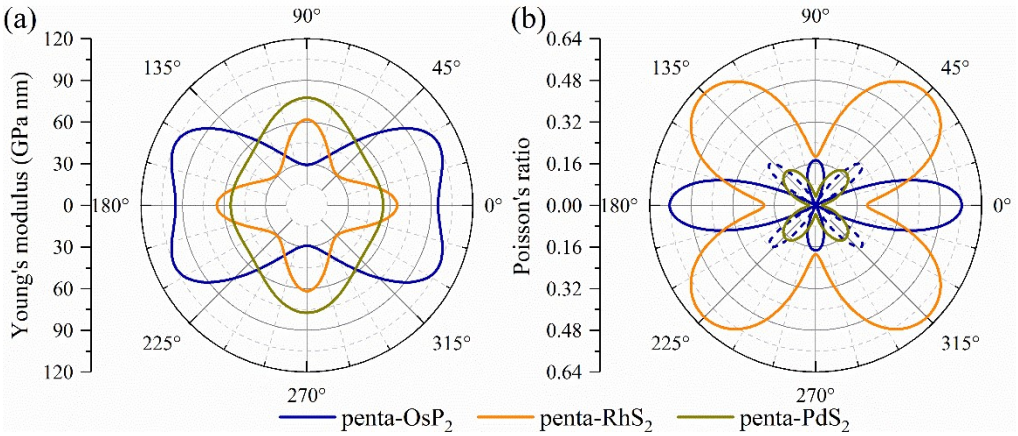

Fig. S3 (a) Young's modulus, and (b) Poisson's ratio of penta-OsP_2, penta-RhS_2, and penta-PdS_2 with respect to the orientation of external stress. The blue dashed lines indicate the negative Poisson's ratio.

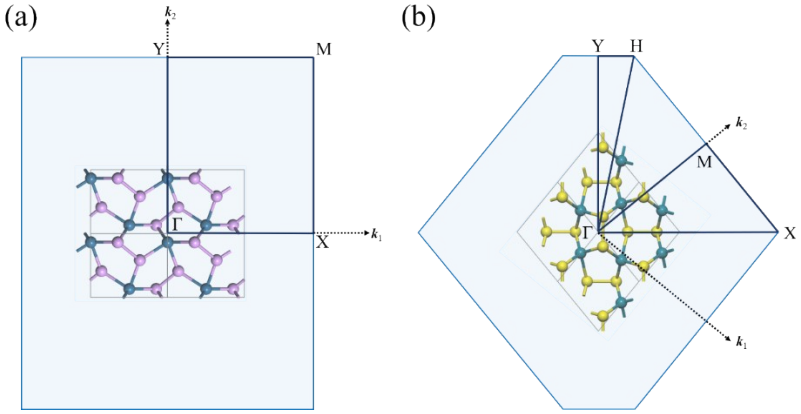

Fig. S4 First Brillouin zone and high-symmetry path of (a) the unit cell of penta-OsP_2 and (b) the primitive cell of penta-RhS_2.

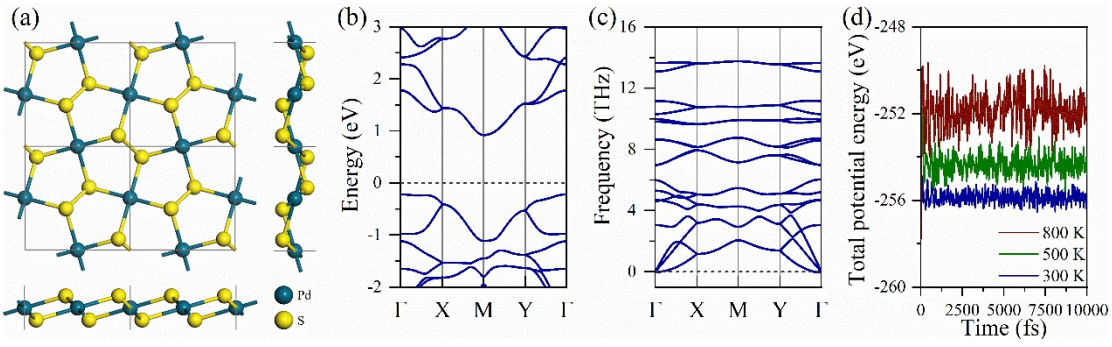

Fig. S5 (a) Geometry, (b) electronic band structure and (c) phonon spectrum of penta-PdS_2. (d) Total potential energy fluctuation of penta-PdS_2 with a 3×3×1 supercell during AIMD simulations.

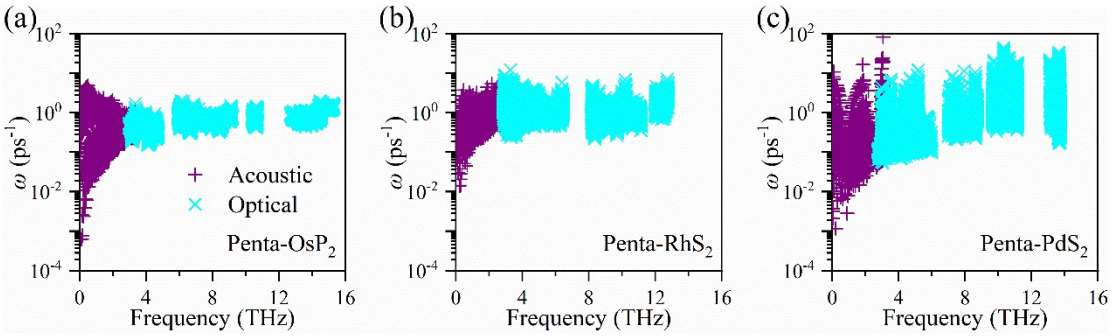

Fig. S6 Overall scattering rate ω of (a) penta-OsP_2, (b) penta-RhS_2, and (c) penta-PdS_2.

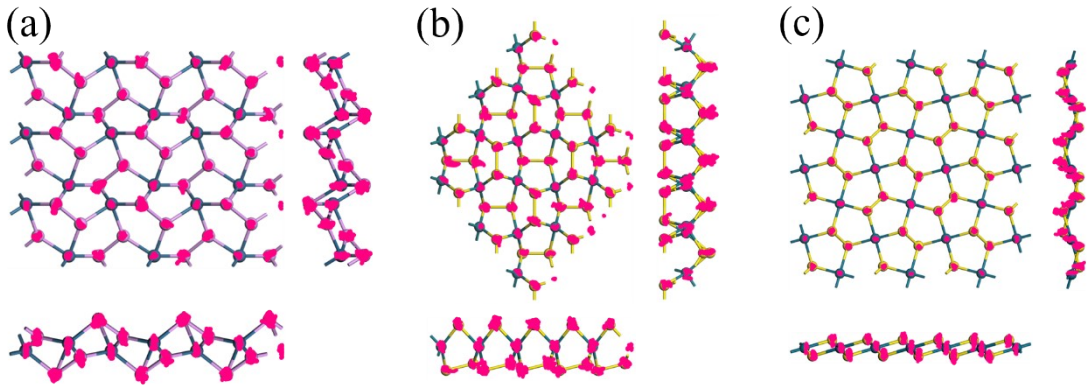

Fig. S7 Trajectory of the atoms in the supercell of (a) penta-OsP_2, (b) penta-RhS_2, and (c) penta-PdS_2 during AIMD simulations at 300 K.

Table S1 Cutoff radii r_{2nd}, r_{3rd} and r_{4th} (in Å) used in the HiPhive fitting in penta-OsP_2, penta-RhS_2 and penta-PdS_2, and the corresponding number of parameters (n_{para}), number of target values (n_{target}), and the goodness of fit (R^2) in the training set and test set, respectively.

Structure	r_{2nd}	r_{3rd}	r_{4th}	n_{para}	n_{target}	R^2_{train}	R^2_{test}
penta-OsP_2	7.8	6.0	3.2	7027	43200	0.99979	0.99969
penta-RhS_2	8.9	6.0	3.2	8740	57600	0.99936	0.99898
penta-PdS_2	10.9	6.0	3.2	2100	17280	0.99998	0.99997

Table S2 Bader charge distribution (in number of electrons) on the atoms in penta-OsP_2 and penta-RhS_2.

penta-OsP_2		penta-RhS_2	
Atom	Bader charge	Atom	Bader charge
$2a_1$ Os	0.02	$4b_1$ Rh	-0.27
$2a_2$ P	-0.03	$4b_2$ S	0.11
$2a_3$ P	0.01	$2a_1$ S	0.18
		$2a_2$ S	0.13

Table S3 Deformation potential E_1 (in eV), effective mass m^* (normalized by the mass of an electron), and the mobility μ (in $cm^2 \cdot V^{-1} \cdot s^{-1}$) of holes and electrons in penta-OsP_2, penta-RhS_2 and penta-PdS_2 along the x and y directions at 300 K.

Structure	Direction	Carrier	E_1	m^*	μ
penta-OsP_2	x	electron	-1.75	0.31	1857.09
	x	hole	-1.52	-0.42	273.64
	y	electron	-3.46	0.79	404.25
	y	hole	-4.11	-11.60	4.86
penta-RhS_2	x	electron	-8.02	2.69	3.59
	x	hole	-4.80	-0.33	180.55
	y	electron	-3.62	4.58	2.99
	y	hole	-6.34	-1.95	26.51
penta-PdS_2	x	electron	-7.72	1.17	25.40
	x	hole	-3.80	-3.74	9.36
	y	electron	-7.17	0.46	67.60
	y	hole	-3.50	-2.13	18.56